J Solid State Electrochem (2005) 9: 750–757
DOI 10.1007/s10008-005-0001-2

ORIGINAL PAPER

Maddalena Corsini · Piero Zanello
Alexander R. Kudinov · Vladimir I. Meshcheryakov
Dmitry S. Perekalin · Konstantin A. Lyssenko

Electrochemical behaviour of cobalta-dicarbollide sandwich complexes with different capping units

Received: 20 December 2004 / Revised: 26 January 2005 / Accepted: 11 February 2005 / Published online: 12 July 2005

Abstract The redox aptitude of a series of cobalt(III) or cobalt(I) sandwich complexes bearing a charge compensated dicarbollide ligand ($[9\text{-L-}7,8\text{-}C_2B_9H_{10}]^-$) as a constant unit and different counterparts (varying from classical $[7,8\text{-}C_2B_9H_{11}]^{2-}$ to charge-compensated $[9\text{-L-}7,8\text{-}C_2B_9H_{10}]^-$ dicarbollides, from cyclopentadienyl $[C_5R_5]^-$ (R = Me, H) to cyclobutadiene $[C_4Me_4]^0$ ligands) has been studied. All the Co(III) complexes display the reversible sequence Co(III)/Co(II)/Co(I). In contrast, the Co(I) complexes (namely, those capped by tetramethylcyclobutadiene) accede reversibly only to the Co(II) oxidation state, the passage to Co(III) being irreversible. When possible, the Co(II) intermediates have been characterized by EPR spectroscopy. The molecular structures of the monocation $[Co(\eta\text{-}9\text{-}SMe_2\text{-}7,8\text{-}C_2B_9H_{10})_2]^+$ in its DD/LL and *meso* diastereomeric forms as well as that of heteroleptic $(\eta\text{-}7,8\text{-}C_2B_9H_{11})Co(\eta\text{-}9\text{-}SMe_2\text{-}7,8\text{-}C_2B_9H_{10})$ have been obtained by single-crystal diffraction.

Introduction

The parallelism between transition metal complexes of the dicarbollide ligand $[C_2B_9H_{11}]^{2-}$ $[M(C_2B_9H_{11})_2]^n$ (n = 1−, 2−) and the corresponding metallocenes is one of the peculiar features of the chemistry of carboranes [1, 2]. In fact, the pioneering discoveries of the similarities between the redox aptitude of $[Fe^{III}\ (C_2B_9H_{11})_2]^-$ and $[Co^{III}\ (C_2B_9H_{11})_2]^-$, and those of ferrocenium and cobaltocenium ions [1, 2] called attention towards the electrochemical behavior of metalla-carboranes [3, 4].

In reality, the early noted isolobal analogy between the open pentagonal faces of $[C_2B_9H_{11}]^{2-}$ and $[C_5H_5]^-$ [5, 6] suffers in principle by the different charge of the two anions, which can reflect on the physico-chemical properties of the two series of complexes. In order to overcome such a flaw, charge compensation procedures have been adopted to produce monoanionic nido-carboranes quite analogues of $[C_5H_5]^-$. Chart 1 shows a few typical examples [7–9].

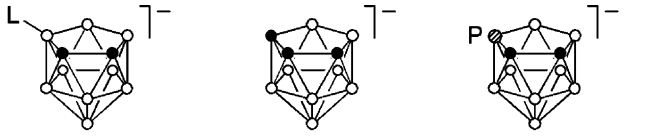

$[9\text{-L-}7,8\text{-}C_2B_9H_{10}]^-$ $[7,8,9\text{-}C_3B_8H_{11}]^-$ $[7,8,9\text{-}PC_2B_8H_{10}]^-$

Chart 1

Chemistry, molecular structures, and electrochemistry of cobaltacarboranes formed from the classical dicarbollide dianion $[7,8\text{-}C_2B_9H_{11}]^{2-}$ or its alkyl carbon substituted derivatives have been widely studied, inclusive not only of bis(dicarbollide) complexes [3, 4, 10–16], but also of those bearing pentagonal half-sandwich units such as cyclopentadienyl [3, 4, 17, 18] or pyrrolyl [19] funtions. In contrast, cobalt complexes of "charge compensated" carboranes are still rare [20–23] with respect to the corresponding iron derivatives [21, 23–30].

In this context, we wish to report here on the electrochemical aspects of the charge-compensated dicarbollide complexes of cobalt illustrated in Chart 2, which bear different half-sandwich capping subunits.

Presented at the 3rd Chianti Electrochemistry Meetings July 3–9, 2004, Certosa di Pontignano, Italy

M. Corsini · P. Zanello
Dipartimento di Chimica dell'Università di Siena,
Via Aldo Moro, 53100, Siena, Italy

A. R. Kudinov (✉) · V. I. Meshcheryakov
D. S. Perekalin · K. A. Lyssenko
A. N. Nesmeyanov Institute of Organoelement Compounds,
28 ul. Vavilova, 119991 Moscow, GSP-1, Russian Federation
E-mail: arkudinov@ineos.ac.ru

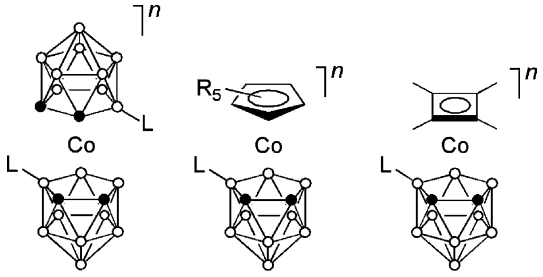

Chart 2

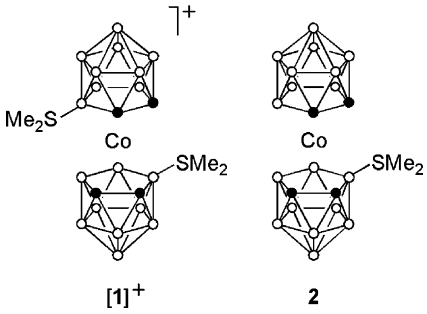

Chart 3

Results and discussion

Let us start with the charge-compensated bis(dicarbollide)-Co^{III} complexes $[Co(\eta\text{-}9\text{-}SMe_2\text{-}7,8\text{-}C_2B_9H_{10})_2]^+$ ($[\mathbf{1}]^+$) and $(\eta\text{-}7,8\text{-}C_2B_9H_{11})Co(\eta\text{-}9\text{-}SMe_2\text{-}7,8\text{-}C_2B_9H_{10})$ (**2**) [31] illustrated in Chart 3.

Cation $[\mathbf{1}]^+$ exists in form of DD/LL and *meso* diastereomers. Their structures were confirmed by X-ray diffraction, Fig. 1.

Both DD/LL- and *meso*-[**1**]BF_4 crystallize with two independent molecules in the unit cell. The independent molecules are practically identical for *meso* form whereas in the case of DD/LL form they differ in rotational conformation of the carborane ligands, the

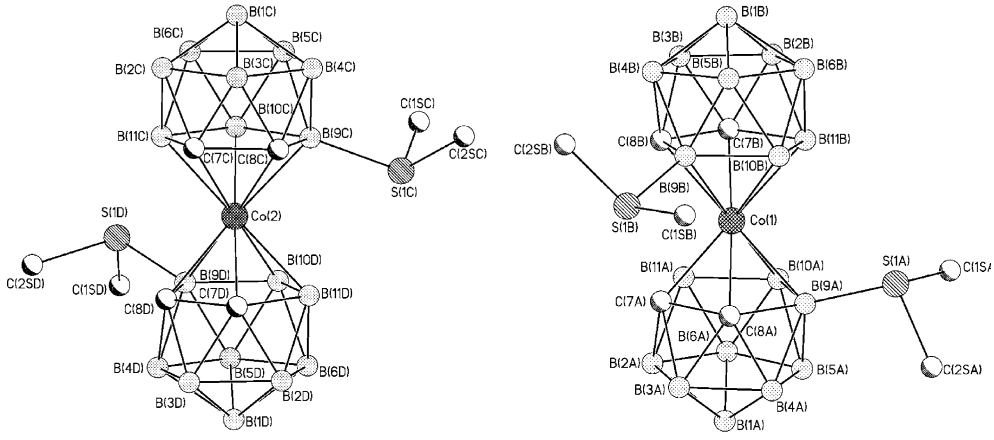

Fig. 1 Structures of cations LL-$[\mathbf{1}]^+$ (left) and *meso*-$[\mathbf{1}]^+$ (*right*), representing one of two independent molecules in each case. The hydrogen atoms are omitted for clarity

Table 1 Selected distances (Å) for *meso*-$[\mathbf{1}]^+$, DD/LL-$[\mathbf{1}]^+$, and **2**

Distance	DD/LL-$[\mathbf{1}]^+$	*meso*-$[\mathbf{1}]^+$	**2**	
	Range; average	Range; average	Substituted carborane ligand	Unsubstituted carborane ligand
C(7)–C(8)	1.609(5)–1.624(5); 1.614	1.611(6)–1.640(6); 1.625	1.618(3)	1.616(3)
C(8)–B(9)	1.676(5)–1.690(5); 1.684	1.692(6)–1.707(6); 1.698	1.687(3)	1.709(3)
B(9)–B(10)	1.777(5)–1.796(5); 1.783	1.738(7)–1.785(7); 1.762	1.792(3)	1.799(3)
B(10)–B(11)	1.794(6)–1.796(6); 1.795	1.791(7)–1.802(7); 1.799	1.807(3)	1.803(3)
B(11)–C(7)	1.665(5)–1.708(6); 1.687	1.685(6)–1.706(6); 1.693	1.706(3)	1.696(3)
B(9)–B(4)	1.779(5)–1.804(5); 1.791	1.768(7)–1.801(6); 1.783	1.788(3)	1.795(4)
B(9)–B(5)	1.759(6)–1.783(6); 1.772	1.749(7)–1.761(7); 1.756	1.778(3)	1.780(3)
S(1)–B(9)	1.909(4)–1.928(4); 1.919	1.907(5)–1.931(5); 1.915	1.921(2)	
Co(1)–C(7)	2.039(3)–2.057(3); 2.047	2.026(4)–2.044(4); 2.032	2.049(2)	2.066(2)
Co(1)–C(8)	2.050(3)–2.069(3); 2.060	2.018(4)–2.042(4); 2.032	2.055(2)	2.053(2)
Co(1)–B(9)	2.085(4)–2.116(4); 2.100	2.091(5)–2.138(5); 2.115	2.092(2)	2.090(2)
Co(1)–B(10)	2.136(4)–2.128(4); 2.121	2.131(5)–2.162(5); 2.152	2.118(2)	2.107(2)
Co(1)–B(11)	2.074(4)–2.093(4); 2.080	2.073(5)–2.115(5); 2.097	2.088(2)	2.088(2)
Co···C_2B_3	1.482–1.492; 1.487	1.485–1.494; 1.489	1.478	1.476

pseudo-torsion angles S(1A)B(9A)B(9B)S(1B) and S(1C)B(9C)B(9D)S(1D) for two rotamers being equal to 175 and 124°. The C–C, C–B, Co–C, and Co–B bond lengths for both DD/LL- and *meso*-$[\mathbf{1}]^+$ cations vary in a rather large range, Table 1, indicating the high flexibility of the framework.

This feature makes the detailed discussion of the intramolecular distances meaningless. Nevertheless, it can be noted that the Co···C_2B_3 distances in cations DD/LL-$[\mathbf{1}]^+$ (1.482–1.492 Å; av 1.487 Å) and meso-$[\mathbf{1}]^+$ (1.485–1.494 Å; av 1.489 Å) are only slightly longer than in the bis(dicarbollide) anionic complex $[Co(\eta\text{-}7,8\text{-}C_2B_9H_{11})_2]^-$ (1.465, 1.475 Å; av 1.470 Å) [32].

The analysis of the crystal packing in DD/LL-$[\mathbf{1}]BF_4$ revealed that the BF_4^- anions form unusually short F···S (F···S 3.068(3)–3.158(4) Å, C–S···F 161–170°) and C–H···F (C···F 3.165(3)–3.301(4) Å, H···F 2.16–2.53 Å, C–H···F 123–167°) contacts with cations, assembling them in layers, Fig. 2, thus suggesting that the charge transfers from the fluorine lone pair to the S–C antibonding orbital. The contact pattern in the crystal of *meso*-$[\mathbf{1}]BF_4$ is quite similar to that observed for DD/LL-$[\mathbf{1}]BF_4$ with contact parameters C···F 2.981(3)–3.347(4) Å, H···F 2.19–2.52 Å, C–H···F 132–163° and F···S 3.104(5)–3.228(5) Å, C–S···F 168.4–173°; however in this case the cations and anions are assembled in a 3-dimensional framework.

The structure of the neutral compound **2**, containing both mono- and dianionic carborane ligands, was also determined by X-ray diffraction, Fig. 3.

Complex **2** crystallizes with one THF molecule which forms rather short intermolecular C–H···O contact with

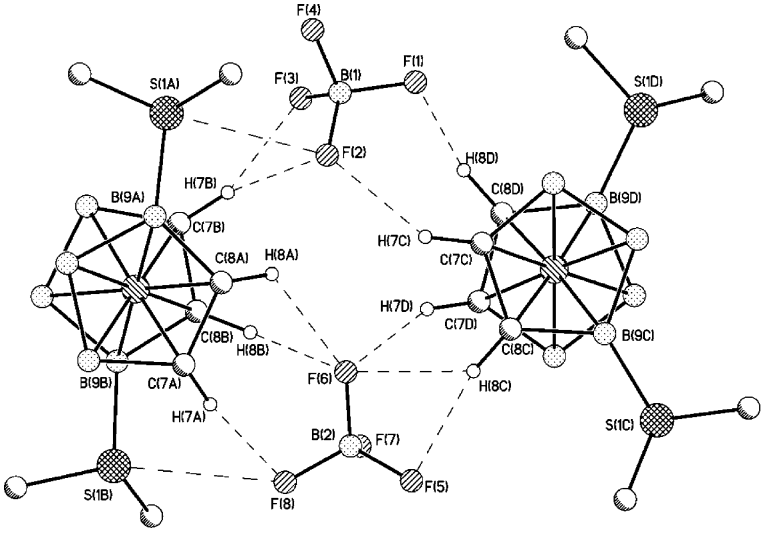

Fig. 2 The fragment of the crystal structure of DD/LL-$[\mathbf{1}]BF_4$ showing the anion-cation interactions. Six top boron atoms of each carborane ligand and the BH hydrogen atoms are omitted for clarity

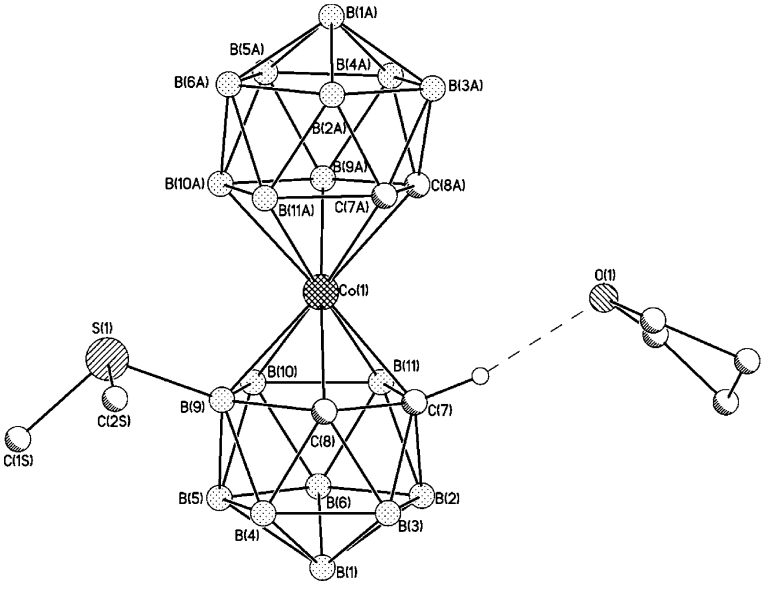

Fig. 3 Structure of **2** showing C–H···O interaction with THF molecule. All hydrogen atoms except H(7) are omitted for clarity

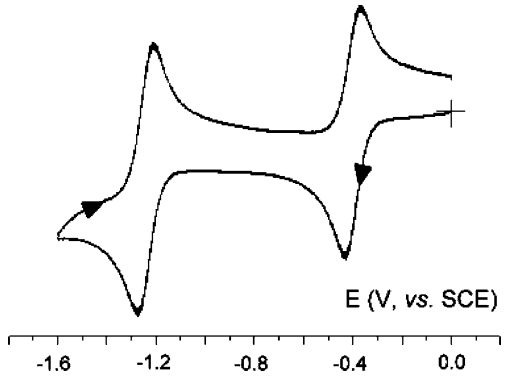

Fig. 4 Cyclic voltammogram recorded at a platinum electrode in CH_2Cl_2 solution of DD/LL-[**1**]$^+$ (0.8×10^{-3} M). $[NBu_4][PF_6]$ (0.2 M) supporting electrolyte. Scan rate 0.2 Vs^{-1}

the CH vertex of the substituted carborane ligand (C(7)···O(1) 3.124(3) Å, H(7)···O(1) 2.08 Å, C(7)–H(7)···O(1) 162°). The Co···C_2B_3 distances are practically the same for both carborane ligands (1.478, 1.476 Å) and are very close to the corresponding values for DD/LL-[**1**]$^+$, *meso*-[**1**]$^+$, and [Co(η-7,8-$C_2B_9H_{11})_2$]$^-$ (vide supra). Thus, the metal-ligand distance is practically independent of the presence of the Me_2S substituent suggesting its insignificant influence on the electron distribution in the metalla-carborane cage.

As illustrated in Fig. 4, which refers to a DD/LL mixture of [**1**]$^+$, all the present bis(dicarbollide)-Co^{III} complexes give rise in CH_2Cl_2 solution to two sequential, chemically reversible, one-electron reductions.

Controlled potential coulometry corresponding to the first reduction (E_w = −0.8 V) consumed one-electron *per* molecule. As a consequence of the exhaustive reduction the original light orange solution (λ_{max} = 466 nm) turns yellow (λ_{max} = 455 nm), and cyclic and hydrodynamic voltammetries [33] afforded responses quite complementary to the original one, thus confirming the stability of the neutral [**1**]^0. Analysis of the pertinent cyclic voltammetric responses with scan rates varying from 0.02 Vs^{-1} to 2.00 Vs^{-1} confirmed the nature of a simple one-electron transfer [33].

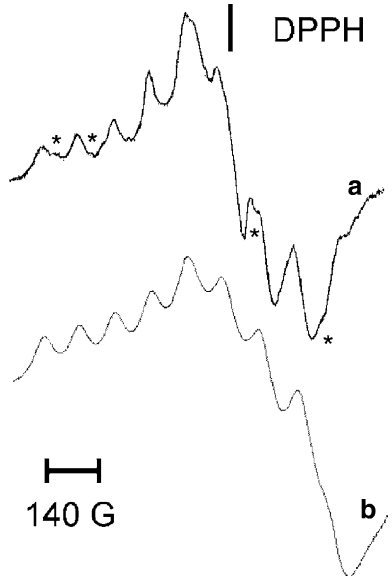

Fig. 5 **a** Experimental X-band EPR spectrum recorded in CH_2Cl_2 solution of electrogenerated [**1**]^0. T = 105 K. **b** Simulated spectrum

In order to confirm that, as happens for the classical [Co^{III} ($C_2B_9H_{11})_2$]$^-$ [2,3], the two reduction processes are cobalt-centred, or involve the sequence Co^{III} /Co^{II} /Co^{I}, EPR spectroscopy on the exhaustively one-electron reduced solution was carried out.

Figure 5a shows the Liquid Nitrogen (T = 100 K) X-band EPR spectrum (first derivative mode) of the electrogenerated [**1**]^0 in CH_2Cl_2 solution. The complex lineshape analysis can be suitably carried out in terms of the S = 1/2 Hamiltonian, taking into account the anisotropic Zeeman and metal hyperfine interactions as basic paramagnetic contributions [34, 35].

Likely due to either the significant Co Spin Orbit coupling constant contribution or the presence of geometrical distortion, the anisotropic signal is very broad even if partially resolved [36]. The appearance of the minor spurious signals (starred peaks) and the intense narrow signal at $g_{average} \cong g_{DPPH}$ testify to the presence of minor paramagnetic impurities, which, as illustrated in Fig. 5b, affect the simulation analysis (in particular in the high-field region) [37, 38]. Notwithstanding, the actual spectrum can be classified as rhombic, with g_i values typical of $3d^7$ Low Spin Co(II) complex: $g_i \neq g_{electron} = 2.0023$, $\lambda_{Co} < 0$, as confirmed by the appearance of the expected cobalt octuplet. (^{59}Co: I = 7/2, natural abundance = 100%), even if accompanied by a significant overlap of the anisotropic signals.

The pertinent computed parameters are: g_l = 2.288(8), g_m = 2.102(8), g_h = 1.988(8), $< g >$ = 2.126(8), a_l(Co) = 70(8)G 100, a_m(Co) = 100(8)G 50, a_h(Co) = 75(8)G 50, $< a >$(Co) = 82(8)G 67.

No evidence for superhyperfine (shpf) magnetic coupling of the unpaired electron with protons (^{1}H: I = 1/2, natural abundance = 99.98%) and boron (^{10}B: I = 3, natural abundance = 19.6%; ^{11}B: I = 3/2, natural abundance = 80.4%) has been gained (an upper limit for such paramagnetic interactions can be evaluated as $a_i(^1H,^{10}B,^{11}B) < \Delta H_i$).

The present spectral features point out the fundamental contribution of the 3d Co A.O.'s to the actual SOMO, and the very minor contributions of the proton and boron orbitals.

With rising temperature, the paramagnetic signal rapidly drops out and at temperatures higher than 165 K the solution becomes EPR mute. Such spectral behavior is not unusual and testifies to the severe effect of thermal contributions to the experimental line widths and the Electron Spin relaxation times.

Refreezing the fluid solution quantitatively restores the rhombic signal, confirming the chemical stability of

Table 2 Formal electrode potentials (V, vs. SCE) for the reduction processes of the bis(dicarbollide)-Co(III) complexes under study and related species

Complex	$E^{o\prime}_{Co(III)/Co(II)}$	ΔE_p^a	$E^{o\prime}_{Co(II)/Co(I)}$	ΔE_p^a	Solvent	Ref.
$[DD/LL\text{-}\mathbf{1}]^+$	−0.37	68	−1.22	72	CH_2Cl_2	b
$[\textit{meso}\text{-}\mathbf{1}]^+$	−0.41	60	−1.24	60	CH_2Cl_2	b
$[\mathbf{2}]^0$	−0.89	80	−1.78	84	CH_2Cl_2	b
$[Co(7,8\text{-}C_2B_9H_{11})_2]^-$	−1.43	≈70[c]	−2.45	≈70[c]	THF	3
$[Co\{(7,8\text{-}C_2B_9H_{11})_2\text{-}C_3N_2H_3\}]^0$	−0.59	–	−1.80	–	MeCN	23

[a]Measured at 0.2 Vs^{-1}; [b]Present work; [c]See Ref. [3]

the paramagnetic $[Co^{II}\ (\eta\text{-}9\text{-}SMe_2\text{-}7,8\text{-}C_2B_9H_{10})_2]^0$ in different experimental conditions.

The formal electrode potentials for the one-electron reductions of the complexes under study are compiled in Table 2, together with those of related complexes.

As shown, charge compensation of the dicarbollide ligands through functionalisation of one of the boron atoms of the coordinating C_2B_3 face, decreasing the overall negative charge, makes the electron addition easier with respect to the classical $[7,8\text{-}C_2B_9H_{11}]^{2-}$. In particular, each $[9\text{-}SMe_2\text{-}7,8\text{-}C_2B_9H_{10}]^-$ ligand facilitates the reduction by about 0.5 V.

Let us now pass to the series of charge-compensated dicarbollide complexes $[(C_5R_5)Co(\eta\text{-}9\text{-}L\text{-}7,8\text{-}C_2R_xB_9H_{10}\text{-}x)]^+$ ($[\mathbf{3a}\text{–}\mathbf{d}]^+$) illustrated in Chart 4.

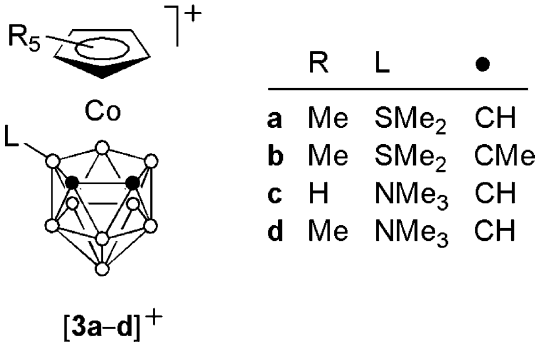

	R	L	●
a	Me	SMe_2	CH
b	Me	SMe_2	CMe
c	H	NMe_3	CH
d	Me	NMe_3	CH

Chart 4

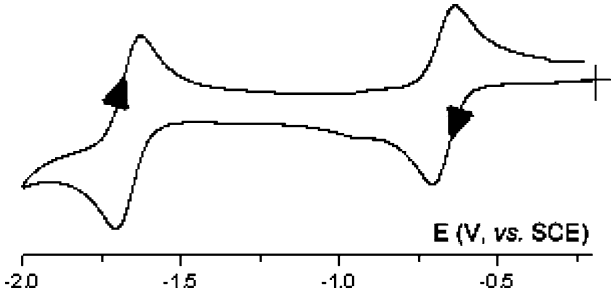

Fig. 6 Cyclic voltammogram recorded at a platinum electrode in CH_2Cl_2 solution of $[\mathbf{3c}]BF_4$ (1.0×10^{-3} M). $[NBu_4][PF_6]$ (0.2 M) supporting electrolyte. Scan rate 0.2 Vs^{-1}

As happens for the previous monocations $[\mathbf{1}]^+$, the present monocations $[\mathbf{3a}\text{–}\mathbf{d}]^+$ undergo two chemically reversible one-electron reductions. Figure 6 representatively shows the cyclic voltammetric behavior of $[\mathbf{3c}]^+$ in CH_2Cl_2 solution.

The formal electrode potentials for the one-electron reductions of the actual monocations are compiled in Table 3, together with those of related complexes.

Apart from the expected higher electron-donating ability of C_5Me_5 vs. C_5H_5, which makes difficult the reduction process of $[\mathbf{3d}]^+$ by 0.2 V with respect to $[\mathbf{3c}]^+$, comparison between $[\mathbf{3a}]^+$ and $[\mathbf{3b}]^+$ shows that insertion of the two electron-donating methyl groups in the carbon atoms of the pentagonal face has little effect on the redox potentials, suggesting that the electron flow to the central cobalt atom is little affected by the carbon atom substituents.

In turn, comparison between $[\mathbf{3a}\text{–}\mathbf{d}]^+$ and $[\mathbf{1}]^+$ (*meso* or racemate forms) indicates that $[9\text{-}SMe_2\text{-}7,8\text{-}C_2B_9H_{10}]^-$ is markedly less electron-donating than $[C_5Me_5]^-$.

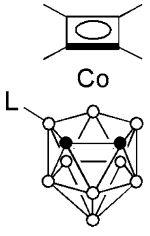

	L	●
a	SMe_2	CH
b	SMe_2	CMe
c	NMe_3	CH
d	py	CH

4a–d

Chart 5

Let us finally pass to the cyclobutadiene complexes $(C_4Me_4)Co(\eta\text{-}9\text{-}L\text{-}7,8\text{-}C_2R_xB_9H_{10}\text{-}x)$ (**4a**–**d**) illustrated in Chart 5.

As a typical example of the structural and electrochemical behavior of such class of compounds, Fig. 7 shows the molecular geometry and the redox activity of complex **4a** [39].

Interestingly, the Co···C_2B_3 distance in **4a** (1.457 Å) is slightly shorter than the corresponding values for the bis(dicarbollide) complexes DD/LL-$[\mathbf{1}]^+$ (av 1.487 Å)

Table 3 Formal electrode potentials (V, vs. SCE) for the reduction processes of the monocations $[\mathbf{3a–d}]^+$ and related species

Complex	$E^{o\prime}_{Co(III)/Co(II)}$	ΔE^a_p	$E^{o\prime}_{Co(II)/Co(I)}$	ΔE^a_p	Solvent	Ref.
$[\mathbf{3a}]^+$	−0.91	62	−1.9[b]	–	CH_2Cl_2	c
$[\mathbf{3c}]^+$	−0.67	68	−1.67	72	CH_2Cl_2	c
$[\mathbf{3d}]^+$	−0.87	64	−1.9[b]	–	CH_2Cl_2	c
$[\mathbf{3b}]^+$	−0.96	60	−1.9[b]		CH_2Cl_2	c
$[(C_5Me_5)Co(\eta\text{-}7,8\text{-}C_2B_9H_{11})]^0$	−1.18	≈70[d]	−1.80	–	THF	3

[a]Measured at 0.2 Vs^{-1};
[b]Peak-potential for irreversible processes;
[c]Present work;
[d]From Ref. [3]

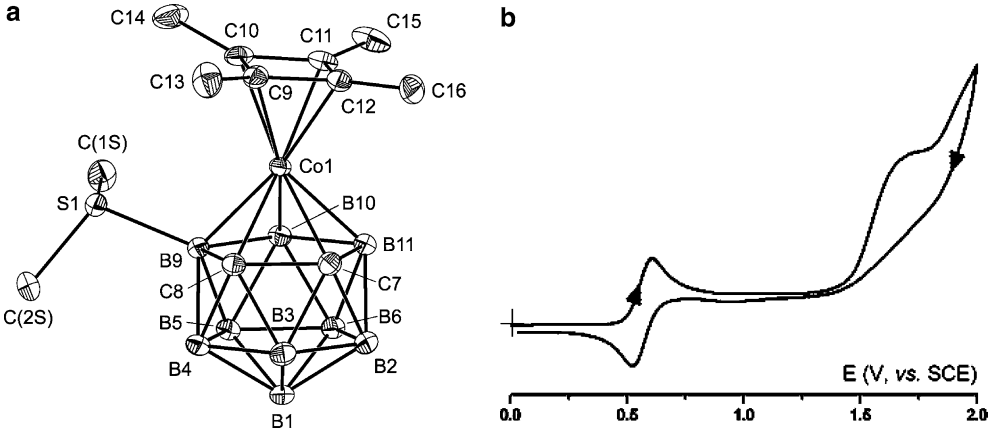

Fig. 7 **a** X-Ray structure of **4a**. **b** Cyclic voltammogram recorded at a platinum electrode in CH_2Cl_2 solution of **4a** (1.3×10^{-3} M). $[NBu_4][PF_6]$ (0.2 M) supporting electrolyte. Scan rate 0.2 Vs^{-1}

and meso-$[\mathbf{1}]^+$ (av 1.489 Å), which is apparently connected with greater back-donation in the case of **4a** due to the electron-donating effect of the Cb* ligand.

Complex **4a** undergoes two sequential oxidation processes, only the first one having features of chemical reversibility. In fact, controlled potential coulometry proved that the first process involves a one-electron removal. The resulting monocation $[\mathbf{4a}]^+$ proved to be quite stable (after exhaustive oxidation, the cyclic voltammetric profile was quite complementary to the original one).

Unfortunately, UV-vis-NIR and EPR spectroelectrochemical measurements carried out upon stepwise oxidation were not conclusive about the original Co oxidation state, in that the UV-vis spectrum simply showed the appearance of a band at $\lambda = 390$ nm attributed to d-d transition. Nevertheless, the EPR features of the spectrum recorded upon one-electron removal, looks compatible with the generation of a low-spin Co(II) derivative [39].

Table 4 Formal electrode potentials (V, vs. SCE) for the oxidation processes of the series **4a–d**

Complex	$E^{o\prime}_{Co(I)/Co(II)}$	ΔE^a_p	$E^b_{p\ Co(II)/Co(III)}$
4a	+0.57	80	+1.7
4b	+0.57	75	+1.4
4c	+0.50	78	+1.6
4d	+0.54	90	+1.6

[a]Measured at 0.05 Vs^{-1};
[b]Peak-potential for irreversible processes

In this light, under the assumption that the original complex has a Co(I) oxidation state, Table 4 summarizes the electrode potentials for the Co(I)/Co(II)/Co(III) sequence.

Comparison between **4a** and **4b** further confirms that the insertion of substituents in the carbon atoms of the dicarbollide ligand does not exert inductive effects on the redox potentials.

As a final consideration, based on the separation of the redox potentials of the sequence Co(I)/Co(II)/Co(III) in all the classes of compounds studied here, one can estimate the stability of the respective Co(II) intermediates towards disproportionation (through the comproportionation constant) [33].

The average values of the disproportionation constant for the complexes illustrated in Charts 3, 4, 5, respectively, are the following:

$$[\text{Co(III)} - \text{bis(dicarbollide)}]$$

$$K_{disp} = 2.9 \times 10^{-15}$$

$$[(\text{cyclopentadienyl})\text{Co(III)}(\text{dicarbollide})]$$

$$K_{disp} = 1.8 \times 10^{-17}$$

$$[(\text{cyclobutadienyl})\text{Co(I)}(\text{dicarbollide})]$$

$$K_{disp} = 3.9 \times 10^{-18}$$

which support the great stability of the different ligand assemblies in the Co(II) oxidation state.

Table 5 Crystal data and structure refinement parameters for complexes DD/LL-[**1**]BF_4, *meso*-[**1**]BF_4, and **2**

Compound	DD/LL-[**1**]BF_4	*meso*-[**1**]BF_4	**2**
Empirical formula	$C_8H_{32}B_{18}CoS_2BF_4$	$C_8H_{32}B_{18}CoS_2BF_4$	$C_6H_{27}B_{18}CoS{\cdot}C_4H_8O$
Formula weight	532.78	532.78	456.95
Crystal colour, habit	light-orange prism	orange prism	orange plate
Crystal size (mm)	0.50×0.40×0.30	0.50×0.45×0.40	0.40×0.10×0.10
Temperature (K)	110(2)	110(2)	100(2)
Crystal system	Monoclinic	Orthorhombic	Triclinic
Space group	$P2_1/n$	$Pna2_1$	P-1
a (Å)	15.031(4)	15.515(2)	6.8357(7)
b (Å)	17.437(6)	30.530(4)	11.369(1)
c (Å)	19.144(7)	10.4775(15)	15.174(2)
α (°)			91.738(2)
β (°)	91.889(7)		95.935(2)
γ (°)			90.516(2)
V (Å^3)	5015(3)	4962.9(12)	1172.3(2)
Z (Z')	8(2)	8(2)	2(1)
F(000)	2160	2160	472
D_{calc} (g cm^{-3})	1.411	1.426	1.295
μ (cm^{-1})	8.80	8.89	8.24
$2\theta_{max}$ (°)	60.00	60.0	60.0
Reflections measured	40722	32965	12622
Independent reflections (R_{int})	14357[0.0671]	14270[0.0383]	6527[0.0324]
Observed reflections [$I > 2\sigma(I)$]	6684	10171	4978
Parameters	778	769	404
R_1 (on F for obs. refls)	0.0623	0.0522	0.0474
wR_2 (on F^2 for all refls)	0.1339	0.0990	0.1005
GOF	1.071	1.038	0.984
$\Delta\rho_{max}$, $\Delta\rho_{min}$ (e Å^{-3})	0.743, −0.587	0.731, −0.422	0.852, −0.534

Experimental

Materials and methods

Synthesis of complex (η-7,8-$C_2B_9H_{11}$)Co(η-9-SMe_2-7,8-$C_2B_9H_{10}$) (**2**) has been carried out according to literature reference [31]. Synthesis of *meso*- and DD/LL-[**1**]BF_4 ([Co(η-9-SMe_2-7,8-$C_2B_9H_{10}$)$_2$]$^+$ ([**1**]$^+$)) will be described elsewhere.

Synthesis and X-ray structures of complexes [**3a–d**]BF_4 {[(C_5R_5)Co(η-9-L-7,8-$C_2R_xB_9H_{10}$-x)]$^+$} will be described elsewhere.

Materials and apparatus for electrochemistry and spectroelectrochemistry [40] and EPR [41] measurements have been described elsewhere. Potential values are referred to the saturated calomel electrode (SCE). Under the present experimental conditions, the one-electron oxidation of ferrocene occurs at $E^{\circ\prime} = +0.39$ V.

X-Ray crystallography

Crystals of complexes *meso*-[**1**]BF_4 and DD/LL-[**1**]BF_4 suitable for X-ray diffraction were grown by slow diffusion in a two-layer system: petroleum ether/solution of complex in acetone-d_6, placed in an NMR tube. Crystals of **2** were grown by slow evaporation of benzene solution. X-Ray diffraction experiments were carried out with a Bruker SMART 1000 CCD area detector, using graphite monochromated Mo-Kα radiation ($\lambda = 0.71073$ Å, ω-scans with a 0.3° step in ω and 10 s per frame exposure) at 110 K. Low temperature of the crystals was maintained with a Cryostream (Oxford Cryosystems) open-flow N_2 gas cryostat. Reflection intensities were integrated using SAINT software [42] and absorption correction was applied semi-empirically using a SADABS program [43]. The structures were solved by direct method and refined by the full-matrix least-squares against F^2 in anisotropic approximation for non-hydrogen atoms. All polyhedron hydrogen atoms were located from the Fourier density synthesis and refined in isotropic approximation. The analysis of the Fourier electron density in the crystal of *meso*-[**1**]BF_4 has revealed that one of the BF_4^- anions is disordered by two positions with occupancies equal to 0.4 and 0.6. Crystal data and structure refinement parameters for DD/LL-[**1**]BF_4, *meso*-[**1**]BF_4, and **2** are given in Table 5.

All calculations were performed using the SHELXTL software [44].

The crystallographic data have been deposited with the Cambridge Crystallographic Data Center, CCDC 257416 for DD/LL-[**1**]BF_4, CCDC 257417 for *meso*-[**1**]BF_4, and CCDC 257415 for **2**. Copies of this information may be obtained free of charge from: The Director, CCDC, 12 Union Road, Cambridge, CB2 1EZ, UK (Fax: +44-1223-336-033; e-mail: deposit@ccdc.cam.ac.uk or http://www.ccdc.cam.ac.uk).

Acknowledgements P.Z. acknowledges the financial support of the University of Siena (PAR 2003). A.R.K. is grateful to General Chemistry and Material Science Division of Russian Academy of Sciences for financial support (Grant No 05–07).

References

1. Hawthorne MF, Young DC, Wegner PA (1965) J Am Chem Soc 87:1818
2. Hawthorne MF, Andrews TD (1965) Chem Commun 443
3. Geiger WE Jr, Bowden WL, El Murr N (1979) Inorg Chem 18:2358
4. Geiger WE Jr (1982) Electrochemistry of metallaboron cage compounds. In: Grimes RN (ed) Metal interactions with boron clusters. Plenum, New York, pp 239–268
5. Brown DA, Fanning MO, Fitzpatrick NJ (1978) Inorg Chem 17:1620
6. Hanusa TP (1982) Polyhedron 1:663
7. Kudinov AR, Perekalin DS, Petrovskii PV, Lyssenko KA, Grintselev-Knyazev GV, Starikova ZA (2002) J Organomet Chem 657:115 and references therein.
8. Holub J, Štibr B, Hnyk D, Fusek J, Cisařová L, Teixidor F, Viñas C, Plzák Z, Schleyer PvR (1997) J Am Chem Soc 119:7750 and references therein
9. Štibr B, Holub J, Bakardjiev M, Hnyk D, Tok OL, Milius W, Wrackmeyer B (2002) Eur J Inorg Chem 2320 and references therein
10. Borodinsky L, Sinn E, Grimes RN (1982) Inorg Chem 21:1686
11. Gomez FA, Johnson SE, Knobler CB, Hawthorne MF (1992) Inorg Chem 31:3558
12. Harwell DE, Nabakka J, Knobler CB, Hawthorne MF (1995) Can J Chem 73:1044
13. Chamberlin RM, Scott BL, Melo MM, Abney KD (1997) Inorg Chem 36:809
14. Viñas C, Pedrajas J, Bertran J, Teixidor F, Kivekäs R, Sillanpää R (1997) Inorg Chem 36:2482
15. Sivaev IB, Bregadze VI (1999) Collect Czech Chem Commun 64:783
16. Teixidor F, Pedrajas J, Rojo I, Viñas C, Kivekäs R, Sillanpää R, Sivaev I, Bregadze V, Sjöberg S (2003) Organometallics 22:3414
17. Hawthorne MF, Young DC, Andrews TD, Howe DV, Pilling RL, Pitts AD, Reintjes M, Warren LF Jr, Wegner PA (1968) J Am Chem Soc 90:879
18. Kaloustian MK, Wiersema RJ, Hawthorne MF (1972) J Am Chem Soc 94:6679
19. Llop J, Viñas C, Teixidor F, Victori L, Kivekäs R, Sillanpää R (2002) Inorg Chem 41:3347
20. Churchill MR, Gold K, Francis JN, Hawthorne MF (1969) J Am Chem Soc 91:1222
21. Kang HC, Lee SS, Knobler CB, Hawthorne MF (1991) Inorg Chem 30:2024
22. Hawthorne MF, Varadarajan A, Knobler CB, Chakrabarti S, Paxton RJ, Beatty BG, Curtis FL (1990) J Am Chem Soc 112:5365
23. Varadarajan A, Johnson SE, Gomez FA, Chakrabarti S, Knobler CB, Hawthorne MF (1992) J Am Chem Soc 114:9003
24. Yan Y-K, Mingos DMP, Müller TE, Williams DJ, Kurmoo M (1994) J Chem Soc Dalton Trans 1735
25. Yan Y-K, Mingos DMP, Müller TE, Williams DJ, Kurmoo M (1995) J Chem Soc Dalton Trans 2509
26. Yan Y-K, Mingos DMP, Williams DJ (1995) J Organomet Chem 498:267
27. Holub J, Grüner B, Cisařová L, Fusek J, Plzák, Teixidor F, Viñas C, Štibr B (1999) Inorg Chem 38:2775
28. Grüner B, Lehtonen A, Kivekäs R, Sillanpää R, Holub J, Teixidor F, Viñas C, Štibr B (2000) Inorg Chem 39:2577
29. Štibr B, Holub J, Bakardjiev M, Pavlík I, Tok OL, Wrackmeyer B (2003) Eur J Inorg Chem 2524
30. Štibr B, Holub J, Bakardjiev M, Pavlík I, Tok OL, Cisařová L, Wrackmeyer B, Herberhold M (2003) Chem Eur J 9:2239
31. Plešek J, Janoušek Z, Heřmanék S (1978) Coll Czech Chem Commun 43:2862
32. Borodinsky L, Sinn E, Grimes RN (1982) Inorg Chem 21:1686
33. Zanello P (2003) Inorganic electrochemistry: theory, practice and application. Royal Society of Chemistry, Cambridge
34. Mabbs FE, Collison C (1992) Electron paramagnetic resonance of d transition metal compounds. In: Studies in inorganic chemistry, vol 16. Elsevier, New York
35. Drago RS (1992) Physical methods for chemists. Saunders College Publishing, New York
36. Bencini A, Gatteschi D (1982) ESR spectra of metal complexes of the first transition series in low-symmetry environments. In: Transition metal chemistry. A series of advances, vol 8. Marcel Dekker Inc., New York
37. Lozos GP, Hoffman BM, Franz CC (1974) QCPE 11:265
38. Romanelli M, Sim. Program GPN1Cu23 (1995) Chemistry Department, Univ. of Florence, Italy
39. Meshcheryakov VI, Kitaev PS, Lyssenko KA, Starikova ZA, Petrovskii PV, Janoušek Z, Zanello P, Corsini M, Laschi F, Kudinov AR (2005) J Organomet Chem (in press)
40. Fabrizi de Biani F, Corsini M, Zanello P, Yao H, Bluhm ME, Grimes RN (2004) J Am Chem Soc 126:11360
41. Zanello P, Laschi F, Fontani M, Mealli C, Ienco A, Tang K, Jin X, Li L (1999) J Chem Soc Dalton Trans 965
42. SMART V5.051, SAINT V5.00 (1998) Area detector control and integration software. Bruker AXS Inc., Madison
43. Sheldrick GM (1997) SADABS, Bruker AXS Inc., Madison
44. Sheldrick GM (1997) SHELXTL V5.10. Bruker AXS Inc., Madison